Hydrophobic gating of mechanosensitive channel of large conductance evidenced by single-subunit resolution

Jan Peter Birkner[a], Bert Poolman[a,b,c], and Armağan Koçer[a,1]

[a]Department of Biochemistry, Groningen Biomolecular Sciences and Biotechnology Institute; [b]Netherlands Proteomics Centre; and [c]Zernike Institute for Advanced Materials, 9747 AG Groningen, The Netherlands

Edited by Ching Kung, University of Wisconsin, Madison, WI, and approved July 5, 2012 (received for review March 28, 2012)

Mechanosensitive (MS) ion channels are membrane proteins that detect and respond to membrane tension in all branches of life. In bacteria, MS channels prevent cells from lysing upon sudden hypoosmotic shock by opening and releasing solutes and water. Despite the importance of MS channels and ongoing efforts to explain their functioning, the molecular mechanism of MS channel gating remains elusive and controversial. Here we report a method that allows single-subunit resolution for manipulating and monitoring "mechanosensitive channel of large conductance" from *Escherichia coli*. We gradually changed the hydrophobicity of the pore constriction in this homopentameric protein by modifying a critical pore residue one subunit at a time. Our experimental results suggest that both channel opening and closing are initiated by the transmembrane 1 helix of a single subunit and that the participation of each of the five identical subunits in the structural transitions between the closed and open states is asymmetrical. Such a minimal change in the pore environment seems ideal for a fast and energy-efficient response to changes in the membrane tension.

duet gene expression | homooligomeric protein | protein engineering

The mechanosensitive channel of large conductance (MscL) from *Escherichia coli* (Eco-MscL) is one of the best-characterized mechanosensitive channels (1, 2). It senses membrane tension invoked by sudden hypoosmotic stress and acts as an emergency valve by opening a large, transient, nonselective aqueous pore in the membrane. The crystal structure of the closed state of MscL from *Mycobacterium tuberculosis* (Tb-MscL) consists of five identical subunits. Each subunit has a helical cytoplasmic N terminus (S1), two transmembrane helices (TM1 and TM2) connected by a periplasmic loop (PL), and a bundle of cytoplasmic helix (CP). The closed channel has a pore diameter of about 3.5 Å (3). The estimated open pore diameter, on the other hand, is 30–40 Å (4, 5), suggesting that significant conformational changes take place upon gating.

Despite a large body of experimental and theoretical data, the gating mechanism by which MscL physically opens and closes its permeation pathway is still unknown. Various molecular rearrangements have been proposed to underlie MscL gating. These include (*i*) a slight counterclockwise (6) or a large clockwise rotation (7) of the TM1 helices when viewed from the periplasm; (*ii*) a significant preexpansion of TM1 helices forming a closed/expanded state followed by separation of S1 bundles (8); (*iii*) the separation of only the TM1 domains but not S1 domains as the primary energy barrier for gating (9, 10); and (*iv*) the rotation and shifting of TM1–TM2 pairs as a rigid body (11, 12).

Despite some discrepancies in details, there are two common elements in all models of MscL gating. The first is a hydrophobic pore constriction formed by a region on TM1 helices. In the crystal structure of Tb-MscL, the pore lumen is lined mainly by TM1 helices, and it narrows toward the cytoplasm. The narrowest part is formed by the fivefold symmetry of a hydrophobic, methyl-terminated motif (L17xxxV21) on TM1 helices (Fig. 1). Random mutagenesis experiments in Eco-MscL identified a similar region of TM1 (L19xxxV23) as the most influential part for channel gating (13). The addition of hydrophilic amino acids to the G22 position in the homopentameric Eco-MscL channel reduced the threshold for opening, whereas hydrophobic additions made the channel harder to open (10). Similarly, in situ labeling of $G22C_5$ homopentamer with a cysteine-specific charged compound [2-(trimethylammonium)ethyl]methanethiosulfonate bromide, (MTSET)] could activate MscL in the absence of applied tension (14). These observations led to the hydrophobic lock hypothesis as a mechanism of MscL gating (9, 10). According to this hypothesis, the hydrophobicity of the pore constriction acts as a functional and/or kinetic block of the gate. As in other gated ion channels with proposed hydrophobic gates (15, 16), MscL also has a structurally open pore constriction in its closed form; functionally, however, it does not conduct ions. During gating, on the other hand, the solvent environment of the hydrophobic residues in the pore constriction changes (10, 17) because of an iris-like movement of TM1 helices, and the channel begins to conduct. According to hydrophobic gating theory, a minor change in the hydrophobicity of the pore lining should be enough to open such channels (15). However, in case of Eco-MscL, because of the homopentameric nature of the channel, the number of TM1 helices required to move to initiate the channel opening is not yet known.

The second common element in MscL gating models is pore opening by an iris-like rotation and tilt of TM helices. However, whether the movement is symmetric or asymmetric is still debated. Given the radial symmetry of the closed structure, early models of gating assumed that tension in the membrane causes symmetric coordinated movement of all subunits during gating (6). However, recent molecular dynamics simulations (18–21) and cross-linking experiments (22, 23) predict an asymmetric cascade of movements initiated by a single TM1 domain leading to full-channel opening.

Here we determined how the channel opening and closing starts. We developed a method that allows us to change the hydrophobicity of Eco-MscL pore lining gradually at a critical position (G22) in one to five subunits so that we could follow the channel behavior at both the ensemble and single-molecule level with single-subunit resolution. Our results demonstrate that (*i*) the hydrophobicity of a single TM1 domain initiates opening and closing of MscL; (*ii*) the participation of the other helices to the channel opening is asymmetric; and (*iii*) the activation of MscL by changing the hydrophobicity of its pore lining causes structural changes similar to those seen in its activation by tension.

Author contributions: J.P.B. and A.K. designed research; J.P.B. performed research; J.P.B., B.P., and A.K. analyzed data; and J.P.B. and A.K. wrote the paper.

The authors declare no conflict of interest.

This article is a PNAS Direct Submission.

[1]To whom correspondence should be addressed. E-mail: a.kocer@rug.nl.

This article contains supporting information online at www.pnas.org/lookup/suppl/doi:10.1073/pnas.1205270109/-/DCSupplemental.

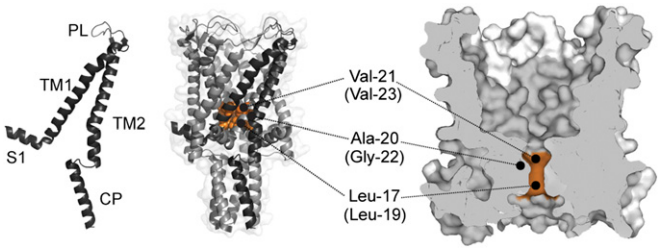

Fig. 1. Structure of MscL. The crystal structure of single subunit (*Left*) and pentameric (*Center*) Tb-MscL [Protein Data Bank (PDB) ID code 2OAR] viewed along the membrane plane and a schematic cross-section through the membrane-embedded part of the protein (*Right*), highlighting the hydrophobic constriction (orange) formed by Leu17 and Val21 (Eco-MscL equivalent residues are Leu19 and Val23). Although physically open, the channel does not conduct ions.

Results

Complex Structure of Homopentameric MscL Can Be Resolved to Individual Subunits. To manipulate the homopentameric channel at a single-subunit level, we developed a method of generating heteropentamers of Eco-MscL from WT and G22C MscL monomers in vivo. The Gly-22 position has been highlighted as the key residue defining the threshold for Eco-MscL activation (10). In our work the G22C mutation serves two functions: It increases the hydrophobicity of the pore lining, because Cys is more hydrophobic than Gly (24), and the cysteine moiety also provides a specific binding site for sulfhydryl-specific small, charged molecules, thus increasing the pore hydrophilicity (Fig. S1).

The cloning and coexpression of two *mscl* genes [encoding for WT MscL with a *StrepII* tag (WT) and for the single-Cys mutant with a His tag (G22C), respectively] in *E. coli* PB104 (25) by using our designed duet expression system, p2BAD, allowed the production of homo- (WT_5 and $G22C_5$) and heteropentameric (WT_4G22C_1, WT_3G22C_2, WT_2G22C_3, and WT_1G22C_4) channel assemblies in the host cell membrane. To purify individual heteropentamers, homopentamers first were separated by using a two-step affinity chromatography procedure. Then individual heteropentamers in the mixture were separated from each other on the basis of their isoelectric points (p*I*). Varying number of His and *StrepII* tags in different heteropentamers changed the overall p*I* value and made it possible to resolve them by chromatofocusing into the expected four fractions (Fig. 2*A*).

The type of heteropentamer in individual fractions was determined by quantification of their G22C and WT subunits. For that quantification, site-directed PEGylation of cysteine residues in each fraction with methoxypoly(ethylenglycol)5000 amidopropionyl methanethiosulfonate (MTS-PEG5000) was followed by separation of the subunits on SDS-PAGE. For high-sensitivity protein detection, all samples also were labeled with an excess of lysine-specific Cy5 before gel loading. The relative protein band intensities of the WT and G22C subunits of a given lane in the gel (Fig. 2*B*) indicated that each fraction indeed contained one of the distinct heteropentamers; the elution order was WT_1G22C_4 (p*I* 7.33 ± 0.02), WT_2G22C_3 (p*I* 7.17 ± 0.02), WT_3G22C_2 (p*I* 6.94 ± 0.02), and WT_4G22C_1 (p*I* 6.65 ± 0.01).

Hydrophobicity of the Pore Constriction in One of Five TM1 Subunits Is Enough to Affect the Gating of MscL. To determine how many subunits per MscL are required to affect the gating of the channel, equal quantities of homo- and heteropentameric MscL were reconstituted individually into large unilamellar vesicles (LUVs) of azolectin, which were loaded with a self-quenching fluorescent dye, calcein (Fig. S3) (26). The gating of MscL under isoosmotic conditions was followed as an increase in the fluorescence signal caused by the release of the dye through MscL pores upon in situ labeling of G22C(s) with a positively charged compound, MTSET (Fig. 3).

LUVs with $G22C_5$ released calcein with a first-order rate constant (k) of 0.825 ± 0.032/min (mean ± SD), whereas the release via WT MscL (WT_5) was not significant (k < 0.001/min). As soon as a single charge was introduced, i.e., by MTSET labeling of WT_4G22C_1, the k increased to 0.216 ± 0.034/min. Further increases in the number of charges per pore increased the first-order k for calcein efflux, albeit in a nonlinear fashion (Fig. 3 and Fig. S4).

To ascertain whether the homo- and heteropentamers are functional, the same channels in LUVs also were activated with their native trigger, membrane tension. For that activation, lysophosphatidylcholine (LPC) (27) was added to the assay system at a constant lipid-to-LPC ratio. We showed that even though WT_5 channels did not release calcein upon MTSET treatment (k < 0.001/min) (Fig. 3), they did release it upon an increase in membrane tension by LPC (k = 0.44/min). Similarly, heteropentamers that show low release in response to MTSET could be activated further by the addition of LPC (Fig. S5). These data show that each of the homo- and heterooligomeric assemblies is fully functional and that the differences in the release profiles in response to MTSET are caused by the different number of WT and G22C subunits per channel.

In contrast to homopentamers, heteropentamers could not be fully activated by tension or charge alone. Even the presence of a single Cys in the channel pore of WT_4G22C_1 made it harder for the mutant to release calcein by a change in membrane tension as elicited by LPC (k = 0.04/min for WT_4G22C_1 compared with 0.44/min for WT_5), whereas charging of its cysteine by MTSET was sufficient for activation (k = 0.17/ min). As the number of G22C subunits, and hence the hydrophobicity, per channel increased further, the magnitude of tension-induced activation decreased. On the other hand, upon charging of an increasing number of G22C subunits with MTSET, and hence increasing hydrophilicity, the charge-induced activation in the absence of tension increased (Fig. S5). These results indicate that minor changes in the hydrophobicity of the pore constriction seem sufficient to alter the probability that the channel is open.

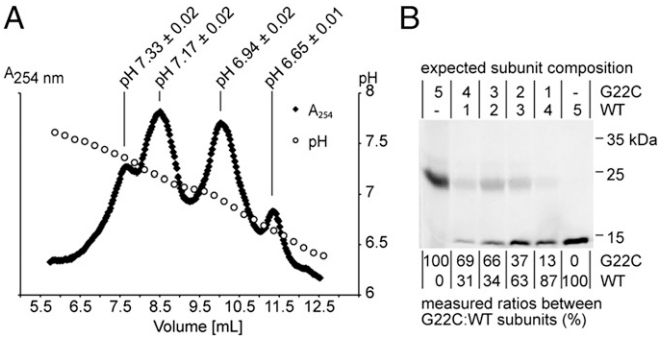

Fig. 2. Heteropentamers of MscL can be separated by chromatofocusing. (*A*) MscL heteropentamers with different numbers of WT-*StrepII* and G22C-*His6* subunits vary significantly in their surface p*I*. The normalized chromatogram shows four peaks representing the individual populations: WT_1G22C_4, WT_2G22C_3, WT_3G22C_2, and WT_4G22C_1 (in the order of their elution from the column). (*B*) Subunit composition of MscL homo- and heteropentamers, determined by site-directed PEGylation and in-gel densitometry. The subunit composition of MscL homo- and heteropentamers after chromatofocusing is shown by in-gel fluorescence of WT and G22C-MTS-PEG5000 subunits labeled with Cy5, and the relative ratio of the subunits within individual fractions was determined by densitometry after calibration with defined amounts of WT and G22C-MTS-PEG5000 homopentamers (Fig. S2).

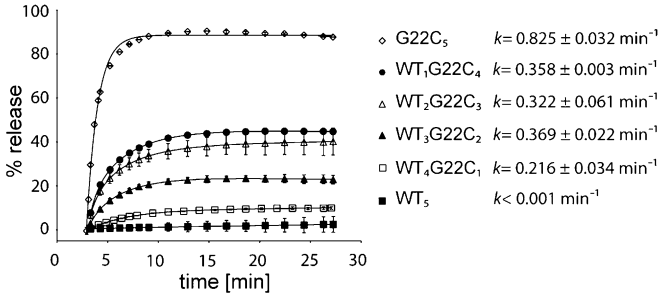

Fig. 3. The number of WT and G22C subunits within a pentamer defines gating properties of MscL in proteoliposomes. Homo- and heteropentamers of MscL were assayed by fluorescence dequenching assays. The net percent release of liposomal content was calculated from the increase in fluorescence. The nonspecific release from liposomes without any MscL was subtracted from that of liposomes with the channel. After the G22C in the pore constriction is charged with MTSET, the hydrophobic lock is disturbed, and calcein can be released through the channel. The initial kinetics and final release correlate directly with the G22C content in pentameric MscL. The first-order rate constants (k) and SD values for calcein efflux are indicated in the figure.

A single hydrophobic residue in the pore constriction is enough to reduce the tension sensitivity of the channel and encourage closing, whereas a hydrophilic residue facilitates the opening.

Hydrophobic Gating at the Single-Molecule Level. To determine the effect of the hydrophobicity of the pore constriction on Eco-MscL gating at the single-molecule level, individual heteropentamers were reconstituted into azolectin LUVs (26), and giant unilamellar vesicles (GUVs) were generated from them by electroformation (28). GUVs were analyzed by patch clamp. The probability of open channels was measured as a function of tension in the membrane, evoked by applying negative pressure to the patch pipette. The channel activation is described by a Boltzmann distribution, which relates the probability of the open channel and negative pressure (29) according to Eq. **1**:

$$P_0/(1-P_0) = \exp[\alpha(p-p_{1/2})] \qquad [1]$$

where P_o is the probability of an open channel, p is the applied negative pressure, $p_{1/2}$ is the negative pressure at which half of the channels are open, and α is the slope of the plot $\ln[P_o/(1-P_o)]$ versus $(p-p_{1/2})$. According to Laplace's law, the tension (t) applied to the membrane will be related directly to the negative pressure ($t = pr/2$). Because pipettes with a tip radius of 1 μm were used in all experiments, we assumed that patches would have equal membrane radii of curvature. Therefore, we used negative pressure in place of tension.

The probability of an open channel of WT and heteropentameric MscL increased with increasing negative pressure. Importantly, with increasing pore hydrophobicity, i.e., with an increased number of G22C subunits per pentamer (Fig. 4 *A* and *B*), the $p_{1/2}$ shifted to higher negative pressures, and the sensitivity of the channel to negative pressure decreased. For instance, WT MscL required 5.59 ± 1.40 mm Hg (mean ± SEM, $n = 3$) negative pressure ($1/\alpha$) for an e-fold increase in the probability of an open channel, consistent with published data (~4.5 ± 2.0 mm Hg, $n = 5$) (4, 30), whereas the presence of a single Cys (WT_4G22C_1) was sufficient to shift the sensitivity to 8.85 ± 0.25 mm Hg ($n = 3$). The tension sensitivity decreased further in a nonlinear fashion with the increasing number of cysteine residues per pentamer (Fig. 4*B*), and for $G22C_5$ the pore could not be opened, because the required tension was beyond the lytic limit of the membranes. Once opened by tension alone, however, the heteropentameric channels showed no significant difference in conductance (Fig. 4*C* and Table S1). These observations indicate that, as in the ensemble measurements, increasing the hydrophobicity of a single TM1 helix at the pore constriction is enough to stabilize its closed state and makes the pore harder to open by tension alone. Further increases in the number of hydrophobic subunits per pentamer magnified the effect, with major steps at one, three, and five hydrophobic residues per pentamer.

To test the effect of increasing the hydrophilicity of the pore constriction at the single-molecule level, MTSET was used to attach positive charges to G22C residue(s), and GUVs were patched in the presence and absence of MTSET with no applied tension. Under these conditions, WT_5 MscL did not conduct any ions. However, as in ensemble measurements, a single charge in the pore, i.e., via MTSET labeling of WT_4G22C_1, was sufficient to observe ion conductance (Fig. 4 *D* and *E*). These channel proteins mainly populated one of the early subconducting states (≤0.5 nS). However, as the number of charges per channel increased (MscL with multiple G22C subunits, labeled by MTSET), the channel gated more frequently, and all the subconducting states known for WT_5 MscL (31) were observed, albeit with a preference for the lower subconducting states (Fig. S6). A detailed analysis of the subconducting state (substate) conductances of homo- and heteropentameric MscLs revealed similar substates for tension- and charge-activated channels (Table S1). These results suggest that MscL follows similar structural rearrangements whether it is activated by tension from the membrane or by the presence of charges in the pore lining.

Application of tension to the charge-activated channels yielded fully open pores (Fig. 4*F* and Fig. S5). Even $G22C_5$ could be opened easily after being labeled with MTSET, whereas tension alone was not sufficient (Fig. 4 *C* and *F*). These results indicate that a charge in the TM1 domain of one of the five subunits in the hydrophobic pore constriction of Eco-MscL is sufficient to lower the energy cost for channel opening and allow the passage of ions independent of tension.

Discussion

Here we provide experimental evidence for hydrophobic and asymmetric gating of MscL. The hydrophobic gating hypothesis was proposed more than a decade ago (15) as one of the gating mechanisms for ion channels and received support mainly from computational studies. It suggests that an unfavorable environment for liquid water inside nanopores creates metastable vapor plugs that functionally block an otherwise physically open pore. The gate can be opened by a minor increase in polarity or radius of the pore. Recently, this principle has been used to generate voltage-gated nonbiological nanopores (32). This gating hypothesis also has been proposed for MscL (9, 10) and found support from molecular dynamics simulations (33) and flying patch clamp studies (34). Our investigation of the strategically engineered MscL provides direct evidence that the hydrophobicity of its pore constriction not only has a structural function in the closed state but also is involved in gating. Our results suggest that under normal conditions the hydrophobicity of this region functionally prevents the passage of ions, even though the crystal structure shows a structurally open pore constriction. However, as soon as there is enough tension in the membrane, the resulting slight movement of a TM1 subunit evokes a change in the hydrophobicity of the pore lining, and this change is enough to initiate the opening of the pore. Similarly, once the channel is open, if one of the TM1 helices moves back and increases the hydrophobicity of the constriction region, it increases the amount of tension required to open the channel, hence encouraging the pore's closing.

The current model of MscL gating describes a symmetric, iris-like movement of all subunits in the transition from closed to open states. However, our results of initiating the gating by one

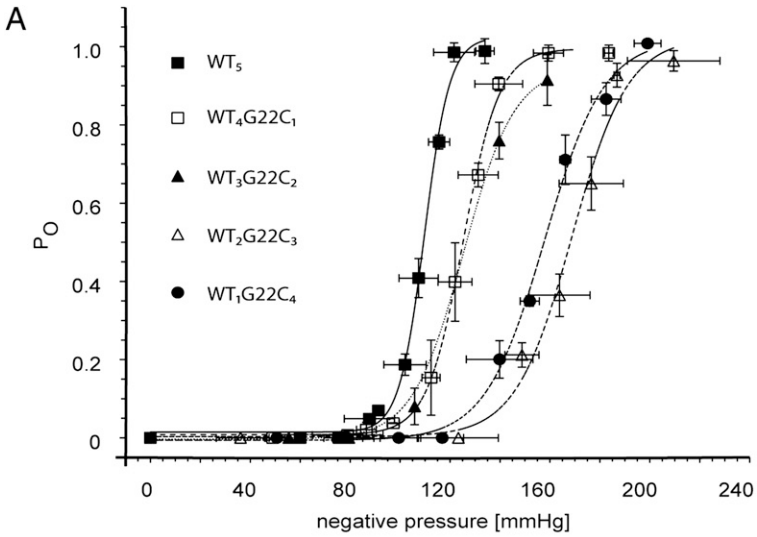

B

	$P_{1/2}$ ± S.E. [mmHg]	1/ α ± S.D. [mmHg]
WT_5	109.75 ± 0.55	5.59 ± 1.40
WT_4G22C_1	125.20 ± 0.37	8.85 ± 0.25
WT_3G22C_2	126.80 ± 0.13	10.83 ± 2.50
WT_2G22C_3	167.96 ± 1.59	12.12 ± 0.02
WT_1G22C_4	157.91 ± 1.24	12.29 ± 3.64
$G22C_5$	N.A.	N.A.

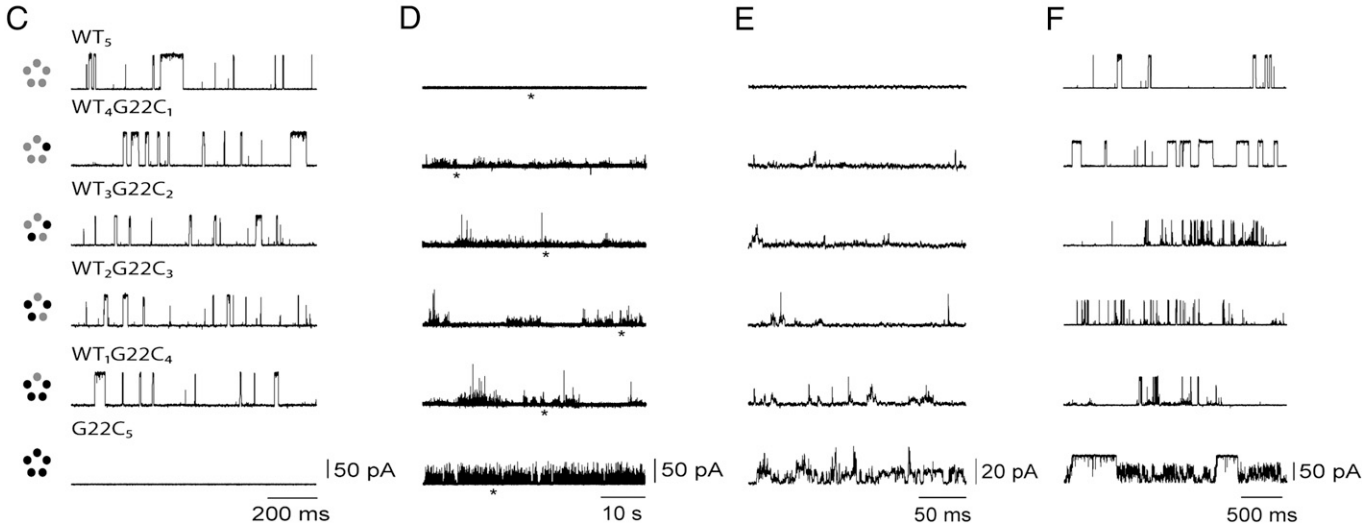

Fig. 4. Probability of an open pore and single-channel conductance of homopentameric MscL and heteropentameric derivatives. (*A*) The probability of an open pore determined from the tension-induced activation of MscL and MscL heteropentamers. As the hydrophobicity of the pore lining increases, the $P_{1/2}$ increases, and the sensitivity to tension decreases. $G22C_5$ could not be activated below the lytic limit of the membrane. (*B*) Gating parameters of homo- and heteropentamers of MscL derived from the fitting of dose–response data in *A* to a Boltzmann distribution function. (*C*) Full opening of MscL channels in patches excised from GUVs when a constant negative pressure of ~100 mm Hg was applied. (*D*) MscL channel activity induced by in situ application of 1.5 mM MTSET into the bath in the absence of applied tension. The channel activity increases with the increasing number of G22C subunits per pentamer. Asterisks mark positions magnified in panel *E* highlighting detailed events of channel gating. (*F*) Channel response upon MTSET treatment and subsequent application of membrane tension by negative pipette pressure. Although the channel response to MTSET treatment alone yields mainly substate activity, the additional application of membrane tension results in full opening of MscL.

subunit and the nonlinear contribution of subsequent subunits to the tension sensitivity provide direct experimental evidence that MscL gating is asymmetric. In addition, these results support the presence of multiple energy barriers with different magnitudes during channel transitions from the closed to the open state (31), but further investigation is needed.

Furthermore, our data revealed that, independent of the trigger (i.e., tension or charge in the pore), the channel visits similar subconducting states, and hence intermediate structures are similar. This observation will pave the way for the use of techniques to explore the gating mechanism of MscL at much earlier stages than patch clamp can provide.

Materials and Methods

p2BAD Construction. p2BAD was constructed by doubling the region from the promoter to the terminator of the parental pBAD-myc-his B plasmid (pBAD24 derivative; Invitrogen) (35) and inserting two multiple cloning sites (MCS). The required construction parts were generated by PCR using pBAD-myc-his B as template. The original MCS was expanded, and nucleotides encoding for a c-*myc* epitope and His tag were removed. Doubling of the promoter-to-terminator region was achieved by inserting the corresponding DNA elements into the parental pBAD-myc-his B plasmid, resulting in the following construction: 5′-MCS1(partial)–Spacer–Transcription Terminator–Promoter–Spacer–ribosomal binding site (RBS)–Spacer–MCS2–Spacer(partial)–3′. The insert resulted in two nearly identical promoter-to-terminator regions. The MCS restriction-recognition sequences and the spacer between RBS and the designated start-codon were different. The resulting p2BAD enables the hosting of two genes, each being expressed from its own ara_{BAD} promoter (Fig. S7).

Duet Expression. Duet expression of *mscL* was carried out in *E. coli* PB104 (25) (*mscL:Cm*^{R}; Ara). $CaCl_2$-competent *E. coli* PB104 cells were transformed with p2BAD WT-*StrepII* G22C-His and were grown in LB medium in the presence of 10 μg/mL chloramphenicol and 100 μg/mL ampicillin. Cells were grown in a bioreactor with pH 7.5, temperature 37 °C, and oxygen control (dissolved oxygen >70%), using a complex medium [12 g/L Bacto-Tryptone (BD), 24 g/L

yeast extract (BD), potassium phosphate (17 mM KH_2PO_4 and 72 mM K_2HPO_4) (pH 7), supplemented with chloramphenicol and ampicillin]. At early and mid-log phases 10 mL of 40% (vol/vol) glycerol/L medium were added as additional carbon source. In the late logarithmic phase of growth, protein expression was induced by adding L-arabinose at 0.1% (wt/vol). Upon induction, another 10 mL 40% (vol/vol) glycerol was added, and cultivation was continued for 90–120 min.

Membrane Vesicle Preparation. Cells were harvested by centrifugation and resuspended in ice-cold 25 mM Tris·HCl, pH 8.0, to a final A_{600} of 100–150. Subsequently, DNase (0.5 mg/mL, final concentration), RNase (0.5 mg/mL, final concentration), and 5 mM $MgSO_4$ were added, and cells were broken using a cell disrupter (Type TS/40; Constant Systems) at 1.7 kbar and 5 °C. Cellular debris was removed by centrifugation for 30 min at 18,460 × *g* and 4 °C. Supernatant was ultracentrifuged at 145,400 × *g* for 90 min at 4 °C. The final supernatant was discarded, and the remaining membrane vesicles were resuspended and homogenized in ice-cold 25 mM Tris·HCl (pH 8.0) to 7 g (wet weight)/mL, corresponding to about 30 mg of protein/mL. Membrane vesicles were frozen in liquid nitrogen and stored at −80 °C.

Protein Isolation. Protein isolation was started using membrane vesicles corresponding to about 60 mg of total protein. Membrane vesicles were solubilized at 5 mg/mL in 50 mM sodium phosphate (pH 8.0), 300 mM NaCl, 1% (vol/vol) Triton X-100, and 35 mM imidazole (solubilization buffer) for 30 min at 4 °C. Unsolubilized material was removed by ultracentrifugation at 267,000 × *g* for 15 min at 4 °C. The supernatant was applied to Ni-NTA agarose resin (Qiagen) [30 mg membrane protein/mL 50% (wt/vol) slurry], equilibrated with 15 column volumes (CV) of solubilization buffer, and incubated under mild agitation for 30 min at 4 °C, enabling binding of the His-tagged proteins to the matrix. Unbound material was collected as flow-through and analyzed when appropriate. The column was washed consecutively with 15 CV wash buffer [50 mM sodium phosphate (pH 8.0), 300 mM NaCl, 0.2% (vol/vol) Triton X-100, 35 mM imidazole] and 7.5 CV L-histidine wash buffer [50 mM sodium-phosphate (pH 8.0), 300 mM NaCl, 0.2% (vol/vol) Triton X-100, 50 mM histidine]. The His-tagged proteins were eluted by addition of 15× 0.25 CV Ni-NTA elution buffer [50 mM sodium phosphate (pH 8.0), 300 mM NaCl, 0.2% (vol/vol) Triton X-100, 235 mM L-histidine]. The protein content of the fractions was checked with the Bradford assay, and all fractions containing protein were combined. Subsequently, the Ni-NTA–purified protein was applied to StrepTactin resin [0.5 mL 50% (wt/vol) slurry/30 mg initial membrane content] (IBA), equilibrated with Ni-NTA elution buffer, and incubated for 30 min with mild agitation at 4 °C to allow binding of *StrepII*-tagged proteins. The remaining supernatant was collected as flow-through, and the resin was washed five times with 2 CV StrepTactin wash buffer [50 mM sodium phosphate (pH 8), 300 mM NaCl, 0.2% (vol/vol) Triton X-100] to remove contaminants. The bound heteropentamers were eluted with 12× 0.25 CV 10 mM biotin buffer [50 mM sodium phosphate (pH 8.0), 300 mM NaCl, 0.2% (vol/vol) Triton X-100, 10 mM biotin] and were analyzed for protein content by the Bradford assay. The fractions with the highest protein content were combined and aliquoted. The total yield of heteropentameric protein was 1.5–2 mg at a final concentration of ∼1 mg/mL MscL. Heteropentamers were frozen in liquid nitrogen and stored at −80°.

Heteropentamer Separation by Chromatofocusing. Heteropentamers of MscL were desalted by using a NAP-10 column, which was equilibrated with chromatofocusing start buffer [25 mM Tris·acetic acid (pH 8.3) at 10 °C, 10 mM NaCl, 0.2% (vol/vol) Triton X-100]. Sample and buffer were used on the day of preparation. The elution buffer for chromatofocusing was prepared as follows: for 100 mL, 7 mL Polybuffer 74, 3 mL Polybuffer 96, 10 mM NaCl, 0.2% (vol/vol) Triton X-100, and MilliQ H_2O. The pH was set to 5.0 with acetic acid at 10 °C. The start and elution buffers were filtered through a 0.2-μm Whatman Membrane Filter (OE66) and were degassed before use.

Chromatofocusing was performed on a Mono P 5/200 GL chromatofocusing column (GE Healthcare), which was washed with filtered and degassed MilliQ H_2O (36). Before sample (1 mL) application, the column was equilibrated with 20 mL start buffer, and a pregradient was formed by washing the column with 6 mL of elution buffer. Protein interaction with the column occurred during the passage of 42 mL eluent for self-gradient formation. During elution, 250-μL fractions were collected. The whole chromatofocusing process was performed at 10 °C in a cold cabinet.

The pH of the fractions was determined at 6 °C using a Sartorius pH meter calibrated at the same temperature. The protein content of the peak fractions was determined by using a 2-D Quant Kit (GE Healthcare) according to the manufacturer's protocol.

Site-Directed PEGylation. For site-directed PEGylation, purified heteropentamers of MscL were incubated for 5 min with β-mercaptoethanol-free SDS/PAGE sample buffer. Then, MTS-PEG5000 (Toronto Research Chemicals, TRC) (10 mM stock in water) was added into the sample to a final concentration of 1.5 mM and mixed. Subsequently, the protein was separated on a 15% SDS/PAGE gel. For quantification of G22C:WT ratios, the gel was scanned using a Fujifilm LAS-3000 imager and was analyzed by using AIDA image analyzing software (Raytest GmbH). For calibration purposes, defined amounts of purified G22C and WT MscL were mixed in weight ratios of 4:1, 3:2, 2:3, 1:4, and 0:1. They were labeled and treated as described above and were applied to the same gel as the sample (Fig. S2).

Lipid Preparation for Reconstitution. Azolectin (soybean; Avanti Polar Lipids) was suspended in lipid buffer (150 mM NaCl, 10 mM sodium phosphate, pH 8.0) to 20 mg/mL by 30-s sonication at room temperature. Subsequently, five freeze–thaw cycles were performed in liquid N_2 and in a water bath at 50 °C. Aliquots of 0.5 mL were stored at −80 °C.

Protein Reconstitution into Preformed Liposomes. Proteins were reconstituted into synthetic liposomes according to Koçer et al. (26). Briefly, azolectin was thawed and homogenized by extrusion 11 times through a 400-nm filter. Liposomes were destabilized by the addition of Triton X-100. Protein and lipids were mixed at 1:50 weight ratio and incubated for 30 min at 50 °C. Subsequently, the appropriate buffer [200 mM calcein in 10 mM sodium phosphate (pH 8.0), 150 mM NaCl for the fluorescence dequenching assay; 10 mM sodium phosphate (pH 8.0), 150 mM NaCl for the patch-clamp measurements] was added in a 1:1 volume ratio and was supplemented with 6 mg (wet weight) Biobeads (SM-2 Absorbents; Bio-Rad) per microliter of detergent (10% Triton X-100) used in the sample and lipid preparation. For detergent removal, the sample was incubated overnight (∼16 h) at 4 °C under mild agitation.

Fluorescence Dequenching Assay. The proteoliposomes were applied on a Sephadex G50 Pharmacia size-exclusion column to remove the free dye. All elution fractions were assayed in a Varian Cary Eclipse Fluorimeter at an excitation wavelength of 495 nm and recording the emission at 515 nm.

In a standard assay (26), 5 μL calcein-filled proteoliposomes were diluted into 2,200 μL efflux buffer. At t = 3 min, MTSET was added at a final concentration of 1 mM. The fluorescence was measured continuously, and the total fluorescence of the sample was determined by dissolving the proteoliposomes by the addition of 0.5% (vol/vol) Triton X-100 at t = 28 min. As a control, the same batch of proteoliposomes was recorded in the absence of MTSET. The datasets were normalized by using the initial fluorescence of each sample as 0% and the signal after the Triton X-100 addition as 100%. Protein content in the liposomes was determined by 12.5% SDS/PAGE (Fig. S3).

In an assay with two channel activators, i.e., MTSET and L-α LPC, 0.75 μL calcein-filled proteoliposomes were diluted into 2,200 μL efflux buffer. Each sample was assayed in two different ways. (*i*) At t = 3 min MTSET was added at a final concentration of 1 mM, and at t = 18 min LPC was added at a final concentration of 4 μM. (*ii*) At t = 3 min LPC was added at a final concentration of 4 μM, and at t = 18 min MTSET was added at a final concentration of 1 mM. The fluorescence was measured continuously, and the total fluorescence of the sample was determined as described above (Fig. S5).

Electroformation and Patch Clamp. GUVs for patch clamp were prepared as described previously (26). Briefly, proteoliposomes were recovered as described for calcein efflux. However, the calcein encapsulation and the size exclusion steps were omitted for patch clamp experiments. Proteoliposomes were diluted to a final lipid concentration of 0.8 mg/mL in 3-(N-morpholino) propanesulfonic acid ·Tris (2 mM, pH 7.5), and 2-μL aliquots were spotted onto the conducting site of an indium tin oxide plate and were dried overnight in a vacuum desiccator at 4 °C.

GUVs were prepared by rehydrating the lipid films in 250 mM sorbitol using the Vesicle Prep Pro instrument (Nanion Technologies). The electroformation protocol was adapted from Girard et al. (37) with AC voltage applied across the cell unit for 3 h with stepwise increases from 0.1–1.1 V at 12 kHz frequency. At the end, to detach glass-attached giant unilamellar liposomes, the AC current was lowered to 4 Hz, and the voltage was raised to 2V for 30 min. Subsequently, GUVs in sorbitol were transferred to a clean tube and assayed by patch clamp.

For patch clamp, the sample chamber of the patch setup was filled with 160 μL of patch buffer (200 mM KCl, 90 mM $MgCl_2$, 10 mM $CaCl_2$, 5 mM Hepes-KOH, pH 7.25) and 5 μL GUV sample (lipid concentration ∼0.44 mg/μL). Calibrated 100-μL pipettes (Drummond Scientific) with a 1-μm tip diameter

were pulled using Sutter Instrument P-1000. The pipette tip was filled with the same buffer as the bath. All recordings were performed with excised patches under the same conditions (20 mV, gain 10, sampling rate of 30 μs). The data were amplified and filtered at 10 kHz using an Axopatch 1D amplifier, sampled at 33 kHz in a Digidata 1322A digitizer, and analyzed with pCLAMP10 software (Molecular Devices).

ACKNOWLEDGMENTS. We thank the MscL Team at the University of Groningen for fruitful discussions, N. Mukherjee for sharing part of her work on the use of lysophosphatidylcholine, and G. T. Robillard for critical reading of the manuscript. This work was supported by the European Research Council-Ideas Program Starting Grant 208814 (to A.K.), the Netherlands Organization for Scientific Research Grant 700.57.427 (to A.K.), and Top-Subsidy Grant 700.56.302 (to B.P.).

1. Sukharev SI, Blount P, Martinac B, Blattner FR, Kung C (1994) A large-conductance mechanosensitive channel in *E. coli* encoded by *mscL* alone. *Nature* 368:265–268.
2. Blount P, Iscla I, Moe PC (2007) *Yuezhou Li. MscL: The Bacterial Mechanosensitive Channel of Large Conductance*, Current Topics in Membranes (Elsevier Inc.), Vol 58, pp 201–233.
3. Chang G, Spencer RH, Lee AT, Barclay MT, Rees DC (1998) Structure of the MscL homolog from *Mycobacterium tuberculosis*: A gated mechanosensitive ion channel. *Science* 282:2220–2226.
4. Cruickshank CC, Minchin RF, Le Dain AC, Martinac B (1997) Estimation of the pore size of the large-conductance mechanosensitive ion channel of *Escherichia coli*. *Biophys J* 73:1925–1931.
5. van den Bogaart G, Krasnikov V, Poolman B (2007) Dual-color fluorescence-burst analysis to probe protein efflux through the mechanosensitive channel MscL. *Biophys J* 92:1233–1240.
6. Sukharev S, Durell SR, Guy HR (2001) Structural models of the MscL gating mechanism. *Biophys J* 81:917–936.
7. Perozo E, Cortes DM, Sompornpisut P, Kloda A, Martinac B (2002) Open channel structure of MscL and the gating mechanism of mechanosensitive channels. *Nature* 418:942–948.
8. Sukharev S, Betanzos M, Chiang CS, Guy HR (2001) The gating mechanism of the large mechanosensitive channel MscL. *Nature* 409:720–724.
9. Blount P, Moe PC (1999) Bacterial mechanosensitive channels: Integrating physiology, structure and function. *Trends Microbiol* 7:420–424.
10. Yoshimura K, Batiza A, Schroeder M, Blount P, Kung C (1999) Hydrophilicity of a single residue within MscL correlates with increased channel mechanosensitivity. *Biophys J* 77:1960–1972.
11. Corry B, et al. (2010) An improved open-channel structure of MscL determined from FRET confocal microscopy and simulation. *J Gen Physiol* 136:483–494.
12. Liu Z, Gandhi CS, Rees DC (2009) Structure of a tetrameric MscL in an expanded intermediate state. *Nature* 461:120–124.
13. Ou X, Blount P, Hoffman RJ, Kung C (1998) One face of a transmembrane helix is crucial in mechanosensitive channel gating. *Proc Natl Acad Sci USA* 95:11471–11475.
14. Yoshimura K, Batiza A, Kung C (2001) Chemically charging the pore constriction opens the mechanosensitive channel MscL. *Biophys J* 80:2198–2206.
15. Beckstein O, Biggin PC, Sansom MSP (2001) A Hydrophobic GatingMechanism for Nanopores. *J Phys Chem B* 105:12902–12905.
16. Beckstein O, Sansom MSP (2006) A hydrophobic gate in an ion channel: The closed state of the nicotinic acetylcholine receptor. *Phys Biol* 3:147–159.
17. Gullingsrud J, Kosztin D, Schulten K (2001) Structural determinants of MscL gating studied by molecular dynamics simulations. *Biophys J* 80:2074–2081.
18. Bilston LE, Mylvaganam K (2002) Molecular simulations of the large conductance mechanosensitive (MscL) channel under mechanical loading. *FEBS Lett* 512:185–190.
19. Kong Y, Shen Y, Warth TE, Ma J (2002) Conformational pathways in the gating of *Escherichia coli* mechanosensitive channel. *Proc Natl Acad Sci USA* 99:5999–6004.
20. Colombo G, Marrink SJ, Mark AE (2003) Simulation of MscL gating in a bilayer under stress. *Biophys J* 84:2331–2337.
21. Louhivuori M, Risselada HJ, van der Giessen E, Marrink SJ (2010) Release of content through mechano-sensitive gates in pressurized liposomes. *Proc Natl Acad Sci USA* 107:19856–19860.
22. Shapovalov G, Bass R, Rees DC, Lester HA (2003) Open-state disulfide crosslinking between Mycobacterium tuberculosis mechanosensitive channel subunits. *Biophys J* 84:2357–2365.
23. Iscla I, Levin G, Wray R, Blount P (2007) Disulfide trapping the mechanosensitive channel MscL into a gating-transition state. *Biophys J* 92:1224–1232.
24. Kyte J, Doolittle RF (1982) A simple method for displaying the hydropathic character of a protein. *J Mol Biol* 157:105–132.
25. Blount P, Sukharev SI, Schroeder MJ, Nagle SK, Kung C (1996) Single residue substitutions that change the gating properties of a mechanosensitive channel in *Escherichia coli*. *Proc Natl Acad Sci USA* 93:11652–11657.
26. Koçer A, Walko M, Feringa BL (2007) Synthesis and utilization of reversible and irreversible light-activated nanovalves derived from the channel protein MscL. *Nat Protoc* 2:1426–1437.
27. Perozo E, Kloda A, Cortes DM, Martinac B (2002) Physical principles underlying the transduction of bilayer deformation forces during mechanosensitive channel gating. *Nat Struct Biol* 9:696–703.
28. Dudia A, Koçer A, Subramaniam V, Kanger JS (2008) Biofunctionalized lipid-polymer hybrid nanocontainers with controlled permeability. *Nano Lett* 8:1105–1110.
29. Hamill OP, Martinac B (2001) Molecular basis of mechanotransduction in living cells. *Physiol Rev* 81:685–740.
30. Häse CC, Le Dain AC, Martinac B (1995) Purification and functional reconstitution of the recombinant large mechanosensitive ion channel (MscL) of *Escherichia coli*. *J Biol Chem* 270:18329–18334.
31. Anishkin A, Chiang CS, Sukharev SI (2005) Gain-of-function mutations reveal expanded intermediate states and a sequential action of two gates in MscL. *J Gen Physiol* 125:155–170.
32. Powell MR, Cleary L, Davenport M, Shea KJ, Siwy ZS (2011) Electric-field-induced wetting and dewetting in single hydrophobic nanopores. *Nat Nanotechnol* 6: 798–802.
33. Anishkin A, Akitake B, Kamaraju K, Chiang CS, Sukharev SI (2010) Hydration properties of mechanosensitive channel pores define the energetics of gating. *J Phys Condens Matter* 22:454120.
34. Petrov E, Rohde PR, Martinac B (2011) Flying-patch patch-clamp study of G22E-MscL mutant under high hydrostatic pressure. *Biophys J* 100:1635–1641.
35. Guzman L-M, Belin D, Carson MJ, Beckwith J (1995) Tight regulation, modulation, and high-level expression by vectors containing the arabinose P_{BAD} promoter. *J Bacteriol* 177:4121–4130.
36. Sluyterman LAA, Elgersma O (1978) Chromatofocusing: Isoelectric focusing on ion-exchange columns, I. General Principles. *J Chromatogr A* 150:17–30.
37. Girard P, et al. (2004) A new method for the reconstitution of membrane proteins into giant unilamellar vesicles. *Biophys J* 87:419–429.